Computation & theory

Validating a mean-field theory via large-scale phase-field simulations for abnormal grain growth induced by nonuniform grain boundary properties

Eisuke Miyoshi[1],* , Munekazu Ohno[2], Yasushi Shibuta[3], Akinori Yamanaka[1], and Tomohiro Takaki[4]

[1] *Division of Advanced Mechanical Systems Engineering, Institute of Engineering, Tokyo University of Agriculture and Technology, 2-24-16 Naka-cho, Koganei-shi, Tokyo 184-8588, Japan*

[2] *Division of Materials Science and Engineering, Faculty of Engineering, Hokkaido University, Kita 13 Nishi 8, Kita-ku, Sapporo, Hokkaido 060-8628, Japan*

[3] *Department of Materials Engineering, The University of Tokyo, 7-3-1 Hongo, Bunkyo-ku, Tokyo 113-8656, Japan*

[4] *Faculty of Mechanical Engineering, Kyoto Institute of Technology, Matsugasaki, Sakyo-ku, Kyoto 606-8585, Japan*

ABSTRACT

The mean-field theory proposed by Humphreys is widely used to predict or interpret abnormal grain growth induced by nonuniform grain boundary properties. Based on this theory, the abnormal growth conditions of a specific grain can be expressed as a function of only three parameters: the size ratio, boundary energy ratio, and mobility ratio between the specific grain and its surrounding matrix grains. However, quantitative and systematic validation of this theory is not yet reported neither in experiments nor simulations. In this study, to elucidate the validity of the mean-field theory, we perform large-scale phase-field simulations for two-dimensional and three-dimensional abnormal grain growth. The multi-phase-field numerical model and parallel graphics processing unit computing are employed, which enables the accurate analyses of abnormal growth in large-scale systems with several hundreds of thousands of grains while accounting for the nonuniformity in grain boundary properties. Systematic simulations are performed while varying the size ratio, boundary energy ratio, and mobility ratio between the specific grain and matrix grains. The simulated results and theoretical predictions on the abnormal grain growth behaviors, i.e., whether or not the abnormal growth occurs and the maximum size that can be reached by an abnormally growing grain, are compared in detail. The large-scale multi-phase-field simulations reveal for the first time the agreement between the mean-field theory and numerical simulation quantitatively, demonstrating that the mean-field theory is a versatile means for describing abnormal grain growth.

GRAPHICAL ABSTRACT
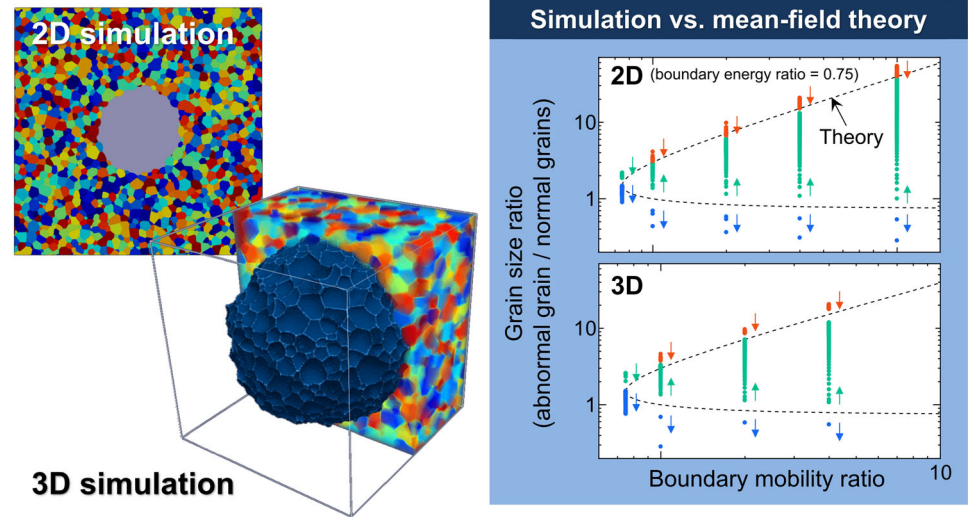
Introduction

During the processing of polycrystalline materials, the competitive growth of crystal grains, i.e., grain growth, is one of the most important metallurgical phenomena, because it determines the final microstructures and resultant physical properties of the materials [1, 2]. Grain growth phenomena can be classified into two categories: normal and abnormal growth. The normal grain growth ubiquitously occurs in the heat treatment of materials, through which the microstructures are coarsened in a uniform manner. On the other hand, the abnormal grain growth is observed only for limited cases; once this phenomenon takes place, a few "abnormal" grains emerge from normally growing grains and undergoes preferential growth. Since the abnormal grain growth plays a decisive role in producing high-performance materials such as textured materials [1, 3] and single crystals [4, 5], the ability to predict the onset and growth behaviors of abnormal grains is of great technological importance.

There are several factors causing abnormal grain growth, including the pinning by second-phase particles [1, 6, 7], surface drag on thin films [8, 9], and nonuniformity in grain boundary properties (energy,

γ, and mobility, M) due to the crystallographic anisotropy and complexion transitions [1, 3, 10–13]. In particular, the abnormal growth induced by nonuniform grain boundary properties is considered the commonest one, being observed in a wide variety of systems from single-phase pure materials to alloys [14–16]. Furthermore, several studies have suggested that this type of abnormal grain growth could be a dominant mechanism for important heat treatment phenomena, e.g., the nucleation of recrystallized grains [10, 17] and texture development [3, 18]. As a simple but useful theory for predicting or interpreting the nonuniform property-induced abnormal grain growth in two-dimensional (2D) and three-dimensional (3D) systems, the mean-field theory proposed by Humphreys [17] is well known. In the mean-field theory, a polycrystalline system is modeled as constituting of two ingredients (see Fig. 1), namely a specific grain with a size R and its surrounding matrix grains with an average size $\langle R \rangle$. Here, all of the grain boundaries of the specific grain are assumed to have a same energy γ and mobility M. Similarly, all the boundaries between the matrix grains take a constant energy $\langle \gamma \rangle$ and mobility $\langle M \rangle$, whose values are different from those of the specific grain (i.e., $\langle \gamma \rangle \neq \gamma$ and $\langle M \rangle \neq M$; this corresponds to the "nonuniformity" in boundary properties). The
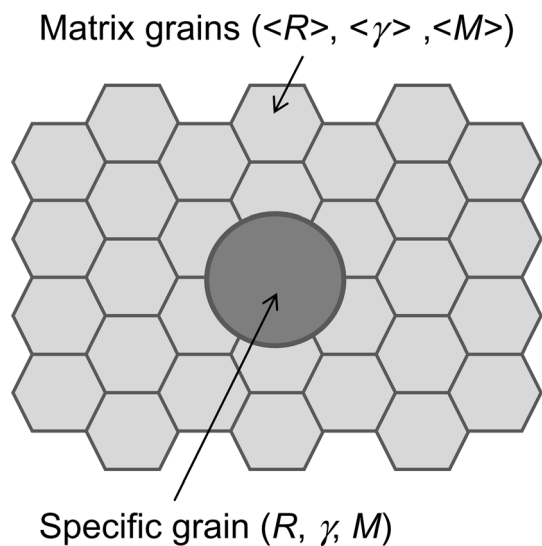
Matrix grains (<R>, <γ> ,<M>)

Specific grain (R, γ, M)

Figure 1 Idealized polycrystalline system for modeling abnormal grain growth. The system consists of a specific grain with a size R and its surrounding matrix grains with an average size $\langle R \rangle$. All of the grain boundaries of the specific grain are assumed to have a same energy γ and mobility M. Similarly, all the boundaries between the matrix grains take a constant energy $\langle \gamma \rangle$ and mobility $\langle M \rangle$, whose values are different from those of the specific grain (i.e., $\langle \gamma \rangle \neq \gamma$ and $\langle M \rangle \neq M$).

growths of the specific grain and matrix grains are all assumed to be purely curvature-driven. Based on this modeling and the mean-field analysis of Hillert [6], the theory allows for predicting the abnormal growth behavior of the specific grain (i.e., whether or not the abnormal growth occurs and the maximum grain size that can be reached when the abnormal growth occurs) using only three parameters: the grain size ratio $\rho = R / \langle R \rangle$, boundary energy ratio $\Gamma = \gamma / \langle \gamma \rangle$, and mobility ratio $\mu = M / \langle M \rangle$. Furthermore, the theory can be easily extended such that it accounts for more complicated metallurgical factors such as particle pinning [19]. We note that Rollett and Mullins [20] published an abnormal grain growth theory independently of Humphreys; although their theory is limited to 2D systems because it is derived from the von Neumann–Mullins law [21], the resultant equations are rather similar to those of the Humphreys theory.

In the original paper of Humphreys [17], he applied the mean-field theory to the analysis of abnormal growth in textured materials, deriving the occurrence conditions of abnormal growth and the maximum size of abnormally growing grains depending on the texture strength (average

misorientation angle of grain boundaries); the analyzed results were proved to be in a qualitative agreement with a few experimental observations [17, 22]. After that, several studies [23–29] have compared the mean-field theory to experimental results for the annealing of pure or alloyed metals and reported that the occurrence of abnormal growth [23, 24, 26, 29, 30] and the limiting sizes of abnormal grains [25–28] seem close to the theoretical prediction. The mean-field theory is therefore considered as a simple but useful framework that can interpret experimental results, and widely employed for analytical/numerical studies of abnormal grain growth and related phenomena [19, 31–36]. However, the previous studies so far have tested the mean-field theory only for limited samples in a qualitative (or semiquantitative) manner, and the systematic and quantitative validation of the theory is still not reported. This is largely attributable to the difficulties in the experimental or numerical verifications of the theory. That is, for experiments, it is not straightforward to prepare an idealized model system (such as that shown in Fig. 1) in specimens and to correctly quantify the characteristics (e.g., sizes) of 3D abnormal grains and their surrounding matrix from usual observations on 2D surfaces or cross sections of the sample. Since computer simulations can easily treat systems with arbitrary geometrical and physical conditions while measuring the 3D characteristic of grains, numerical investigations on abnormal grain growth are frequently attempted based on continuum-based grain growth models, including the Monte Carlo [10, 13, 37, 38], cellular automaton [39], phase-field [40–43], and level-set [44] models. However, in a usual computational scale employed to date ($\sim$ several hundreds or thousands of grains), sufficiently long-term observation of abnormal grain growth is not feasible, and therefore, it is difficult to compare the maximum size reached by the abnormal grains with the theoretical predictions. To quantitatively elucidate the validity of the classical mean-field theory, very large-scale simulations of abnormal growth should be achieved.

Lately, there have been great advances in grain growth simulation using the phase-field model: The multi-phase-field (MPF) models developed in several works [45–49] and the active parameter tracking (APT) algorithm proposed by three groups [50–52] allowed for the effective computation of grain growth while avoiding the artificial coalescence of grains.

The MPF models were also proved to accurately handle grain boundary migrations under nonuniform boundary properties [53, 54]. Moreover, thanks to recent developments in high-performance computing, very large-scale phase-field simulation is becoming possible. For instance, by enabling massively parallel graphics processing unit (GPU) computing on a supercomputer, our previous studies achieved large-scale phase-field simulations on various solidification phenomena [55–59]. Very recently, we have applied the parallel GPU computing to a MPF model [48], and succeeded in simulating 3D normal grain growth with an extra-large number (orders of 10^5–10^6) of initial grains [60–62]. This computational scale allowed for correctly quantifying the statistical behaviors of normal grain growth. These findings suggest that large-scale MPF simulation will also provide a prominent means for describing the abnormal grain growth induced by nonuniform boundary properties with statistical and numerical accuracy.

Given the above background, we aim to elucidate for the first time the validity of the mean-field theory of abnormal grain growth [17] through comparison to very large-scale MPF simulations. As a first step, this study mainly focuses on 2D abnormal growth that is computationally easy to handle, and systematically investigates the effects of the size ratio $\rho = R/\langle R \rangle$, boundary energy ratio $\Gamma = \gamma/\langle \gamma \rangle$, and mobility ratio $\mu = M/\langle M \rangle$ on the abnormal growth behaviors. Although computational scales such as the time duration of simulations are limited, we also attempt the evaluations on 3D abnormal growth. The remainder of this paper is organized as follows: First, in Sect. 2, the mean-field theory of abnormal grain growth is briefly outlined. Next, Sect. 3 describes the methodology and computational conditions for MPF grain growth simulations. The parallel GPU scheme [60–62] is applied to abnormal grain growth, enabling systematic simulations on greatly enlarged scales. In Sect. 4, we discuss the validity of the mean-field theory based on the simulations. While varying the initial size ratio, boundary energy ratio, and mobility ratio between matrix grains and a potentially abnormal grain, 2D and 3D simulations are systematically performed and compared to the theoretical predictions. Finally, in Sect. 5, we conclude this paper with a summary and some remarks on future work.

Mean-field theory of abnormal grain growth

We briefly describe the mean-field theory of abnormal grain growth proposed by Humphreys [17]. Let us again consider the model system shown in Fig. 1 that consists of a specific grain (size R, grain boundary energy γ, and mobility M) and its surrounding matrix grains (average size $\langle R \rangle$, grain boundary energy $\langle \gamma \rangle$, and mobility $\langle M \rangle$). Here, grain sizes R and $\langle R \rangle$ are defined as the circle-equivalent radii for 2D and sphere-equivalent radii for 3D. Note that this "specific grain" can be interpreted as a kind of a statistical outlier. That is, the sizes of grains in actual materials have a distribution, where a minority of very large grains typically have a size around 2.5–3 times larger the average grain size [1]. Similarly, the orientations of grains are also distributed. A few grains whose orientations are significantly different from the preferred orientation of other grains will exhibit unique grain boundary properties. Such grains with statistically significant differences from other grains correspond to "specific" ones.

In the mean-field theory, the following assumptions for grain boundary properties are used for simplification:

(1) Grain boundary energy and mobility are dependent solely on the boundary misorientation angle (i.e., inclination dependencies are omitted, which is because the misorientation is typically significantly more dominant on the variations in the boundary properties [63, 64]).

(2) Grain boundaries constituting the specific grain take a uniform misorientation angle, θ. Similarly, the boundaries between the matrix grains also take a uniform misorientation, $\langle \theta \rangle$. In actual materials, of course, θ and $\langle \theta \rangle$ have distributions, but the mean-field theory simplifies the situation by using the average values as the representative values.

(3) Grain boundary energy and mobility of the specific grain, γ and M, and those between the matrix grains, $\langle \gamma \rangle$ and $\langle M \rangle$, which depend on the misorientation angles, are also constant for the specific grain boundaries and for the matrix grain boundaries, respectively.

Therefore, the explicit parameters to describe the thermodynamic conditions of a system are γ, $\langle \gamma \rangle$, M, $\langle M \rangle$. Using this modeling, the abnormal growth

conditions for the specific grain can be expressed as a function of the grain size ratio $\rho = R/\langle R \rangle$, boundary energy ratio $\Gamma = \gamma/\langle \gamma \rangle$, and mobility ratio $\mu = M/\langle M \rangle$, as demonstrated below.

With the assumption that the grain growth is driven only by grain boundary curvatures, the derivation of the Humphreys theory is done using two basic equations for describing curvature-driven kinetics. One is the mean-field approximation for individual grain growth kinetics, through which the growth rate of the specific grain, dR/dt, is determined by its size R relative to the average (mean) size $\langle R \rangle$ of the matrix grains:

$$\frac{dR}{dt} = \alpha M\left(\frac{\langle \gamma \rangle}{\langle R \rangle} - \frac{\gamma}{R}\right) \Leftrightarrow R\frac{dR}{dt} = \alpha M\langle \gamma \rangle(\rho - \Gamma), \quad (1)$$

where α is a geometrical constant that takes a value of 0.5 for 2D and 1 for 3D systems. Equation (1) can be regarded as an intuitive expansion of Hillert's mean-field equation [6], $dR/dt = \alpha M\gamma (1/\langle R \rangle - 1/R)$, to the case of nonuniform grain boundary energy ($\gamma \neq \langle \gamma \rangle$). The other basic equation is that describing the growth rate of the average size of the matrix grains, which is given by the well-known parabolic law [6]:

$$\frac{d\langle R \rangle}{dt} = \frac{\alpha}{4}\frac{\langle M \rangle \langle \gamma \rangle}{\langle R \rangle} \quad \Leftrightarrow \quad \frac{d\langle R \rangle^2}{dt} = \frac{\alpha}{2}\langle M \rangle \langle \gamma \rangle. \quad (2)$$

The growth rate of the specific grain relative to that of the matrix grains, $d\rho/dt$, can be expressed as:

$$\frac{d\rho}{dt} = \frac{d}{dt}\left(\frac{R}{\langle R \rangle}\right) = \frac{1}{\langle R \rangle^2}\left(\langle R \rangle\frac{dR}{dt} - R\frac{d\langle R \rangle}{dt}\right). \quad (3)$$

By substituting Eqs. (1)–(2) to Eq. (3) and re-arranging it, $d\rho/dt$ reduces to:

$$\begin{aligned}\frac{d\rho}{dt} &= \frac{\alpha\langle M \rangle \langle \gamma \rangle}{R\langle R \rangle}\left[-\frac{1}{4}\left(\frac{R}{\langle R \rangle}\right)^2 + \frac{M}{\langle M \rangle}\frac{R}{\langle R \rangle} - \frac{M}{\langle M \rangle}\frac{\gamma}{\langle \gamma \rangle}\right] \\ &= \frac{\alpha\langle M \rangle \langle \gamma \rangle}{R\langle R \rangle}\left[-\frac{1}{4}\rho^2 + \mu\rho - \mu\Gamma\right]\end{aligned} \quad (4)$$

As first shown by Thompson et al. [65], when $d\rho/dt > 0$, the specific grain will grow faster than the normally growing matrix grains and lead to the occurrence of abnormal grain growth. Hence, the abnormal growth condition for the specific grain is:

$$X \equiv -\frac{1}{4}\rho^2 + \mu\rho - \mu\Gamma > 0. \quad (5)$$

Furthermore, the two roots of $X = 0$ determine the lower and upper bounds of the abnormal growth:
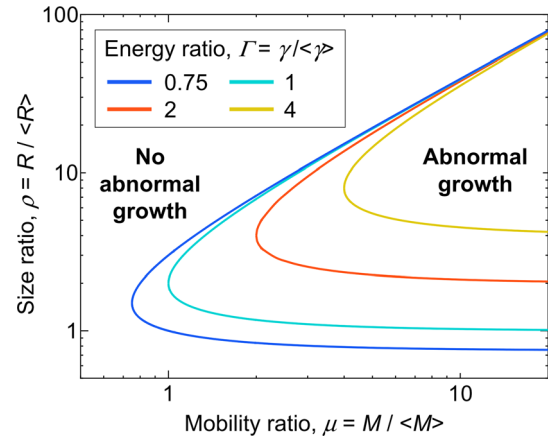
Figure 2 Abnormal growth conditions of the specific grain shown in Fig. 1 as a function of the grain size ratio $\rho = R/\langle R \rangle$, boundary energy ratio $\Gamma = \gamma/\langle \gamma \rangle$, and mobility ratio $\mu = M/\langle M \rangle$. If the specific grain has a relative size ρ larger than the lower bound of a solid curve (i.e., minimum size ratio ρ_{min} given by Eq. (6)), it will undergo the abnormal growth and grow to the upper bound of the curve (i.e., maximum size ratio ρ_{max} given by Eq. (7)). For the conditions where $\mu < \Gamma$, ρ_{min} and ρ_{max} do not have real number values and the specific grain always shrinks for any ρ value.

$$\rho_{min} = 2\mu - 2\sqrt{\mu(\mu - \Gamma)}, \quad (6)$$

$$\rho_{max} = 2\mu + 2\sqrt{\mu(\mu - \Gamma)}. \quad (7)$$

The condition for abnormal grain growth therefore depends on $\rho = R/\langle R \rangle$, $\Gamma = \gamma/\langle \gamma \rangle$, and $\mu = M/\langle M \rangle$. This relation can be illustrated as a diagram shown in Fig. 2. As shown in Fig. 2, if the specific grain has a relative size ρ larger than the lower bound of a solid curve (i.e., minimum size ratio ρ_{min}), it will undergo the abnormal growth and grow to the upper bound of the curve (i.e., maximum size ratio ρ_{max}). When the abnormal grain attains the maximum size ratio ρ_{max}, it continues to grow, but the ratio ρ remains constant. For the conditions where $\mu < \Gamma$, as confirmed from Eqs. (6)–(7), ρ_{min} and ρ_{max} do not have real number values and the specific grain always shrinks for any ρ value.

When analyzing abnormal grain growth using the mean-field theory, the grain boundary energies and mobilities are often expressed as functions of misorientations using the Read–Shockley relation and the sigmoidal model, respectively, as Humphreys himself did in his original paper. However, many studies have reported that, in real materials, these boundary properties frequently deviate from the description of the existing models such as the Read–Shockley and

sigmoidal ones [66–68], and conclusive models are not yet established. Therefore, in the rest of this paper, the grain boundary properties are not expressed by specific functions, but are treated as independent parameters that can be set arbitrarily.

Simulation methodology

Multi-phase-field model

The MPF model proposed by Steinbach and Pezzolla [48] is employed for grain growth simulations, because it can effectively and accurately handle grain boundary migration under nonuniform boundary energy and mobility [54]. This model represents a polycrystalline system including N grains through N phase-field variables ϕ_i ($i = 1, 2, \ldots, N$), which take a value of 1 in the ith grain, 0 in the other grains, and $0 < \phi_i < 1$ at the grain boundaries. The sum of the phase-field variables at any spatial point in the system should be conserved as:

$$\sum_{i=1}^{N} \phi_i = 1. \tag{8}$$

When considering pure curvature-driven grain growth, the total free energy of the system, G, is expressed as:

$$G = \int_V \sum_{i=1}^{N} \sum_{j=i+1}^{N} \left(W_{ij} \phi_i \phi_j - \frac{a_{ij}^2}{2} \nabla \phi_i \cdot \nabla \phi_j \right) dV, \tag{9}$$

where W_{ij} and a_{ij} denote the barrier height and gradient coefficient of the boundary between the ith and jth grains, respectively. The migration of grain boundaries is reproduced by calculating the time evolution of ϕ_i at each spatial point under the constraint of the minimization of G. The time evolution equation satisfying Eq. (8) is given as:

$$\frac{\partial \phi_i}{\partial t} = -\frac{2}{n} \sum_{j=1}^{n} M_{ij}^{\phi} \sum_{k=1}^{n} \left\{ (W_{ik} - W_{jk}) \phi_k + \frac{1}{2} \left(a_{ik}^2 - a_{jk}^2 \right) \nabla^2 \phi_k \right\}, \tag{10}$$

where n denotes the number of coexisting grains at the spatial point and M_{ij}^{ϕ} denotes the phase-field mobility of the boundary between the ith and jth grains. In the simulations that follow, the n value was

evaluated using the iterative algorithm of Takaki et al. [69], which allows for accurate and stable MPF computation of grain growth with nonuniform grain boundary properties [54].

The parameters M_{ij}^{ϕ}, W_{ij}, and a_{ij} included in Eq. (10) are related to the thickness (δ), energy (γ_{ij}), and mobility (M_{ij}) of the grain boundary through the following equations:

$$M_{ij}^{\phi} = \frac{\pi^2}{8\delta} M_{ij}, \quad W_{ij} = \frac{4\gamma_{ij}}{\delta}, \quad a_{ij} = \frac{2}{\pi} \sqrt{2\delta\gamma_{ij}}. \tag{11}$$

In the simulations that follow, for the grain boundaries constituting the specific grain (Fig. 1), γ_{ij} and M_{ij} are set to uniform values of γ and M, respectively. On the other hand, for the grain boundaries between the matrix grains, constant values of $\langle \gamma \rangle$ and $\langle M \rangle$ are used for γ_{ij} and M_{ij}, respectively.

The boundary thickness δ must be large enough to resolve the boundary regions. Here, we set δ to six times the grid spacing, which has been reported as a good compromise between computational accuracy and cost [50]. The time evolution equation (Eq. (10)) was numerically solved using the first-order forward difference scheme and second-order central difference scheme for time and space, respectively.

Computational systems and parameters

To elucidate the validity of the mean-field theory of abnormal grain growth, a series of large-scale MPF simulations were performed and compared to the theory. Since, as shown later (Sect. 4), it is difficult to analyze the long-term behaviors of 3D abnormal growth even using the current high-performance computing technique, we mainly focused on 2D grain growth and thoroughly examined the phenomenon via systematic simulations. However, a few simulations were also performed on 3D grain growth for the basic evaluation of the mean-field theory for 3D cases. The computational conditions we employed for the 2D and 3D simulations are summarized below. Note that the units for time, length, grain boundary energy, and mobility are all nondimensionalized with typical scales of 1 s, 10^{-6} m, J/m^2, and 10^{-12} m^4/(Js), respectively.

Conditions for abnormal grain growth simulations

Figure 3 depicts the computational systems for simulating 2D/3D abnormal grain growth, which consist of a circular/spherical specific grain of size R and approximately 300,000 (2D) or 200,000 (3D) matrix grains with an average size of $\langle R \rangle$. The 2D and 3D domains with periodic boundaries were divided into $12,288^2$ and 1280^3 grid points, respectively, using regular square grids of size $\Delta x = 1$.

To examine the effects of the initial size ratio $\rho_{init} = (R/\langle R \rangle)_{init}$, boundary energy ratio $\Gamma = \gamma/\langle \gamma \rangle$, and mobility ratio $\mu = M/\langle M \rangle$ on the abnormal growth behavior of the specific grain, systematic simulations were carried out while varying these parameters. Here, the initial average size $\langle R \rangle_{init}$, boundary energy $\langle \gamma \rangle$, and mobility $\langle M \rangle$ of the matrix grains were set to $\langle R \rangle_{init} = 12.2$ (2D) or 12.5 (3D), $\langle \gamma \rangle = 1$, and $\langle M \rangle = 1$, whereas those of the specific grain were varied. Note that when $\Gamma < 0.5$ for 2D and $\Gamma < \sqrt{3} \approx 0.6$ for 3D, the specific grain infinitely grows due to the occurrence of solid-state wetting [70]; therefore, we limited Γ to range ≥ 0.75. In addition, as grain boundary mobilities in actual materials generally exhibit stronger nonuniformity than boundary energies [67, 71], the mobility ratio μ was set within a wider range than energy ratio, as follows: $\mu = 0.75$–10 and $\Gamma = 0.75$–4 for 2D, and $\mu = 0.75$–4 and $\Gamma = 0.75$–2 for 3D. Here, for 3D simulations that are computationally much more expensive than 2D simulations, we limited the Γ and μ values to relatively narrow ranges. This is because, as stated below (Eq. (12)), the time increment Δt for the simulations must decrease with increasing Γ and μ values, and accordingly, the computational cost of 3D simulations with large Γ and μ is tremendously high. Note that within the range of nonuniformity in the grain boundary properties employed here, the MPF model can accurately reproduce the grain boundary migration rate (with errors less than several percent), as shown in a previous study [54]. As mentioned in Sect. 2, when $\mu < \Gamma$, abnormal growth is not expected to occur for any ρ value. In such cases, the initial size ratio ρ_{init} was set to 4. By contrast, for cases where $\mu > \Gamma$, the following three conditions were used for the ρ_{init} value.

- $\rho_{init} = 0.67 \times \rho_{min}$: the specific grain is initially smaller than the minimum relative size, ρ_{min}, given by Eq. (6) and is expected to shrink.

- $\rho_{init} = 1.33 \times \rho_{min}$: the specific grain is initially larger than ρ_{min}, expected to grow abnormally to the maximum relative size, ρ_{max}, given by Eq. (7). In this case, for most Γ and μ values, the specific grain has an initial size of 1–3 times the average size of the matrix grains, which is within the typical range of the maximum grain size observed in actual materials [1]. Only for $\Gamma = 4$ with $\mu = 10$, the initial relative size of the specific grain ($R \approx 6 \langle R \rangle$) is outside the typical range.

- $\rho_{init} = 1.33 \times \rho_{max}$: the specific grain is initially larger than ρ_{max}, expected to grow, but decrease its relative size to ρ_{max}.

The above-described conditions for ρ_{init} and μ are schematically illustrated in Fig. 4 and compared to the abnormal grain growth diagram shown in Fig. 2. Here, as an example, we set the Γ value to 1. The simulations started with the conditions shown in Fig. 4.

The time increment, Δt, of the simulations was determined from the stability condition for the explicit schema, as follows:

$$\Delta t = 0.75 \frac{\Delta x^2}{\beta M_{max} \gamma_{max}}, \quad (12)$$

where β is a parameter that takes a value of 4 for 2D cases and 6 for 3D cases. $\gamma_{max} = \max\{\gamma, \langle \gamma \rangle\}$ and $M_{max} = \max\{M, \langle M \rangle\}$ are the maximum values of the boundary energies and mobilities in the system, respectively. The Δt value is hence dependent on the conditions of the boundary property ratios, Γ and μ.

For each simulation, the initial polycrystalline structures were created as follows: First, a polycrystalline structure with 600,000 (2D) or 685,000 (3D) matrix grains was prepared in the computational domain by growing randomly distributed nuclei under a constant driving force. The resultant structure is equivalent to that obtained by the Voronoi tessellation. Then, to avoid an artificial effect coming from the use of the Voronoi structure, a normal grain growth simulation was conducted for 2000 time steps, after which 284,728 (2D) or 190,960 (3D) grains remained in the system. Finally, a specific grain with a circular/spherical shape was embedded in the center of the computational domain. The initial structures for each simulation were the same, except for the initial size of the specific grain.

As summarized here, the initial size advantage of the specific grain was arbitrarily set in the
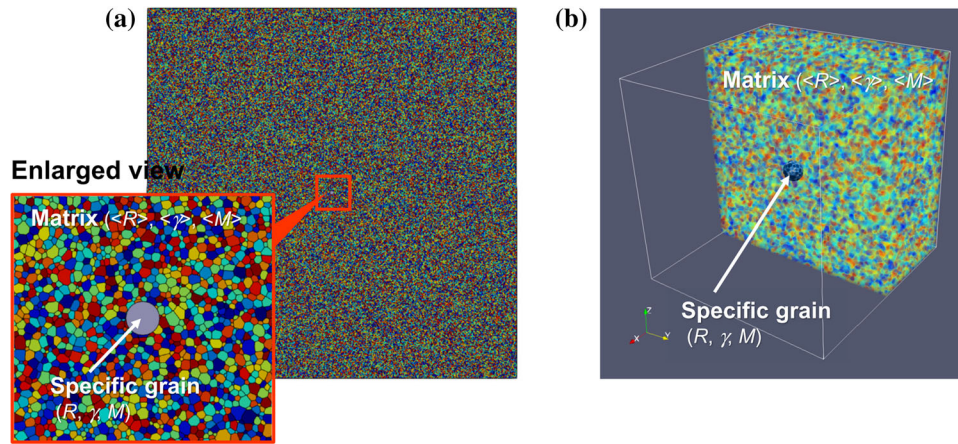
Figure 3 Polycrystalline systems used for simulating 2D and 3D abnormal grain growth. **a** 2D system with $12{,}288^2$ grid points, which consists of a circular specific grain (size R, boundary energy γ, boundary mobility M) and approximately 300,000 matrix grains (average size $\langle R \rangle$, boundary energy $\langle \gamma \rangle$, boundary mobility $\langle M \rangle$). **b** 3D system with 1280^3 grid points, which consists of a spherical specific grain and approximately 200,000 matrix grains. In all panels, grains are distinguished by different colors according to the IDs assigned to each grain. In panel (**b**), the matrix grains are visualized only for the region with X-coordinate < 640 to make the specific grain visible.
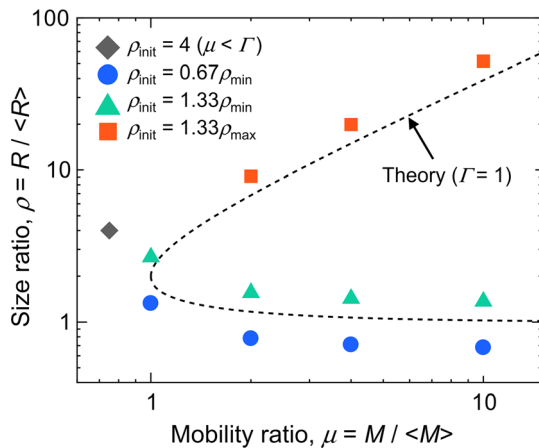

Figure 4 Schematic of the computational conditions (ρ_{init} and μ) used in the abnormal grain growth simulations for $\Gamma = 1$. The dashed line indicates the abnormal growth condition of the specific grain predicted by Humphreys theory.

simulations. However, it should be noted that the methods to obtain this size advantage are of great interest in metallurgy. Although several formation mechanisms of the initial large grains have been suggested (e.g., the rapid growth of a few nuclei formed at very early stages during phase transformation [72], dissolution of second-phase particles and the resulting unpinning of particular grains [73], and coalescence of subgrains in deformed materials [1, 74]), the details of their formation are still debated. The formation mechanisms of potentially abnormal grains will be addressed elsewhere. In addition,

according to the simple Humphreys model, the present simulations account for only two types of grain ingredients (specific/matrix grains) without inclination-dependent boundary properties, which results in nearly circular or spherical abnormally growing grains (see Fig. 5 in Sect. 4). By contrast, abnormal grains observed in actual samples frequently exhibit more anisotropic and irregular shapes [4, 16, 44, 75]. To elucidate the formation mechanism of such irregularly shaped abnormal grains, multiple complex factors need to be considered, including more than two types of grain ingredients and strong anisotropy of the grain boundary properties [41, 76, 77]. The simple system addressed in this study is expected to be helpful for such endeavors because it establishes a benchmark for quantifying the effect of complex factors.

Computational environment

To perform the large-scale simulations which enable the detailed comparison of the simulations and the mean-field theory, we utilized our own CUDA C code [60, 78] that was developed for parallel GPU computation of the MPF model. The code decomposes an entire computational domain into small subdomains, each of which is assigned to one GPU. The connection of the boundary data of the GPUs is performed via their host CPUs [55], while the internode communication is implemented using the

message-passing interface (MPI). To reduce the memory requirements, the APT algorithm [50–52] of Kim et al. [50] was employed, storing only nonzero phase-field variables; the maximum number of stored variables at each grid point was set to seven. All the simulations were carried out on the GPU-rich supercomputer TSUBAME3.0 at the Tokyo Institute of Technology, using 16 GPUs (NVIDIA Tesla P100) for the 2D simulations and 64 GPUs for the 3D simulations.

Results and discussion

Using the above-mentioned computational conditions, we performed many of the 2D abnormal grain growth simulations for a period of 2,200,000 time steps, within which the grain size ratios, $\rho = R/\langle R \rangle$, were observed to reach almost constant (limiting) values. For the conditions where the boundary energy ratio, $\Gamma = \gamma/\langle \gamma \rangle$, and mobility ratio, $\mu = M/$

$\langle M \rangle$, are larger than unity, simulations were continued for longer durations (4,000,000–12,000,000 steps), because the time increment Δt must be set to relatively small values for these conditions (see Sect. 3.2.1). 3D simulations were conducted until 250,000 time steps; by this time, the specific grain reached the boundaries of the computational domain in many of the simulations, and therefore, correct analyses on the abnormal growth behaviors of the specific grain became difficult. The performed simulations are more than ten times larger in time and space (the number of grids and initial grains) than the previously largest 2D and 3D abnormal grain growth simulations [13, 39, 41, 76].

As examples of the evolved microstructures obtained from the simulations, Fig. 5 depicts the microstructures for the conditions of $\Gamma = 0.75, 2$ with $\mu = 4$, as obtained in (a) 2D simulations at dimensionless time $t = 92,750$ (2,000,000Δt for $\Gamma = 0.75$; 4,000,000Δt for $\Gamma = 2$) and (b) 3D simulations at $t = 3906.25$ (125,000Δt for $\Gamma = 0.75$; 250,000Δt for

Figure 5 Evolved microstructures for the conditions of $\Gamma = 0.75, 2$ with $\mu = 4.0$, as obtained in **a** 2D simulations at dimensionless time $t = 92,750$ (2,000,000Δt for $\Gamma = 0.75$; 4,000,000Δt for $\Gamma = 2$) and **b** 3D simulations at $t = 3906.25$ (125,000Δt for $\Gamma = 0.75$; 250,000Δt for $\Gamma = 2$). The initial structures for the simulations are those shown in Fig. 3 with the initial relative size $\rho_{ini} = 1.33\rho_{min}$ or $1.67\rho_{min}$. In all panels, grains are distinguished by different colors according to the IDs assigned to each grain. In panel (**b**), the matrix grains are visualized only for the region with X-coordinate < 640 to make the specific grain visible.
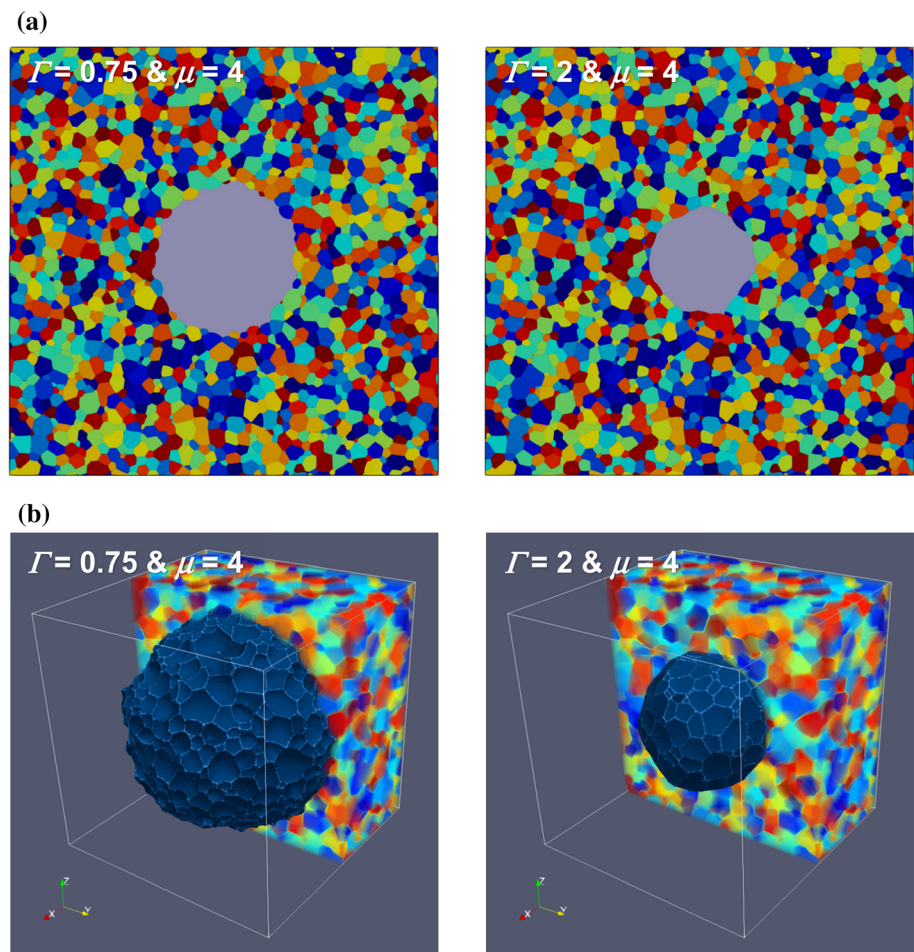
$\Gamma = 2$). The initial structures are those shown in Fig. 3. In both the panels of Fig. 5, we can see that the matrix grains are coarsened in a uniform manner and generally exhibit equiaxed shapes, into which the abnormally growing specific grains encroach. Overall, the simulated microstructural evolutions exhibit a typical picture of abnormal grain growth. In addition, in contrast with the case of $\Gamma = 2$, large local curvatures in each boundary face shared by the specific grain and its neighboring matrix grains are observed for $\Gamma = 0.75$. Further, the boundary faces form relatively sharp contact angles at the triple junctions. This indicates that the grain boundaries migrated such that mechanical balance was maintained at their junctions in accordance with Young's law; hence, the nonuniformity in the grain boundary properties was reflected in the current MPF simulations. In the following, based on the calculated results, we present quantitative comparisons between the simulations and mean-field theory of abnormal grain growth, focusing particularly on the limiting relative sizes that the specific grain reached and whether the abnormal growth occurs or not.

Comparison of the theoretical and simulation results

This section investigates the 2D and 3D abnormal grain growth behaviors using systematic simulation results. First, we focused on the temporal variations and limiting values of the grain size ratio, $\rho = R/\langle R \rangle$, between the specific grain and matrix grains. Figure 6 shows, as typical examples, the simulated temporal variations in ρ for the (a) 2D system with energy ratio $\Gamma = 2$ and mobility ratios $\mu = 4$–10 and (b) 3D system with $\Gamma = 2$ and $\mu = 4$, where the simulations started from different initial ρ values ($\rho_{\text{init}} = 1.33\rho_{\text{min}}$ and $1.33\rho_{\text{max}}$). The limiting values of ρ (i.e., ρ_{max}) predicted from the theory are also shown in Fig. 6 as dashed lines. Note that the cross mark in panel (b) indicates the termination of the simulation because the specific grain reached the boundaries of the computational domain. The mean-field theory predicts that abnormal growth of a specific grain occurs (i.e., $\mathrm{d}\rho/\mathrm{d}t > 0$) for $\rho_{\text{init}} = 1.33\rho_{\text{min}}$ and does not occur ($\mathrm{d}\rho/\mathrm{d}t < 0$) for $\rho_{\text{init}} = 1.33\rho_{\text{max}}$, in both of which ρ approaches its limiting value, ρ_{max}. In Fig. 6, as expected, ρ gradually converges to a constant value near the theoretically predicted ρ_{max} values in most of the simulations, although relatively large

deviations from the theory are observed for $\rho_{\text{init}} = 1.33\rho_{\text{min}}$ compared to the case of $\rho_{\text{init}} = 1.33\rho_{\text{max}}$ (the reason for this is discussed in the next section). The exceptions are the results for the condition of $\rho_{\text{init}} = 1.33\rho_{\text{min}}$ with $\mu = 4$ in 2D (left-hand panel of Fig. 6) and 3D (Fig. 6b), where the specific grains do not abnormally grow, but shrink and eventually disappear, in contrast to the theoretical predictions. For these cases, we performed additional simulations using a slightly larger initial relative size of $\rho_{\text{init}} = 1.67\rho_{\text{min}}$. The additional simulations showed that, as exhibited in Fig. 6, $\rho_{\text{init}} = 1.67\rho_{\text{min}}$ results in abnormal grain growth, consistent with the mean-field theory, with the ρ value converging to the theoretically predicted ρ_{max}.

As shown in Fig. 6, the degree of convergence of the ρ versus time curves varies depending on the conditions. For instance, in the right-hand panel of Fig. 6a (2D system with $\Gamma = 2$ and $\mu = 10$), while the result for $\rho_{\text{init}} = 1.33\rho_{\text{max}}$ almost perfectly converges to a constant value after some duration, the convergence of the result for $\rho_{\text{init}} = 1.33\rho_{\text{min}}$ appears to be relatively incomplete, despite the large spatiotemporal scale of the current simulations. The incomplete convergence of ρ is more pronounced in the 3D simulation results shown in Fig. 6b. To quantitatively determine the completeness and incompleteness of the convergence of ρ, we defined the following simple criteria:

$$\Delta\rho_{\text{rel}}(t, \ t_{\text{end}}) = \frac{\rho(t) - \rho(t_{\text{end}})}{\rho(t_{\text{end}})}, \tag{13}$$

$$\min\{\Delta\rho(t, \ t_{\text{end}}) \mid t < t_{\text{c}}\} \begin{cases} < \varepsilon : & \text{complete convengence}, \\ \geq \varepsilon : & \text{incomplete convergence}, \end{cases} \tag{14}$$

where $\Delta\rho_{\text{rel}}(t, t_{\text{end}})$ denotes the relative change in ρ between time t and end time t_{end} of the simulation, t_{c} denotes a certain time sufficiently distant from t_{end}, and ε denotes the tolerance for convergence. Thus, if a ρ value very close to $\rho(t_{\text{end}})$ is observed at a time t far from t_{end}, the result is regarded as converged. Here, we set t_{c} to $4/5$ of the entire simulation period, and ε to 0.01 (1%). As examples for the determination of the convergence of ρ, Fig. 7 shows the temporal variations in $D\rho_{\text{rel}}(t, t_{\text{end}})$ compared to those in ρ with different initial size ratios ρ_{init}, as obtained for the 2D simulation results at $\Gamma = 2$ and $\mu = 10$ shown in the right-hand panel of Fig. 6a. As shown in Fig. 7a, for the case of $\rho_{\text{init}} = 1.33\rho_{\text{min}}$, $\Delta\rho_{\text{rel}}(t, t_{\text{end}})$
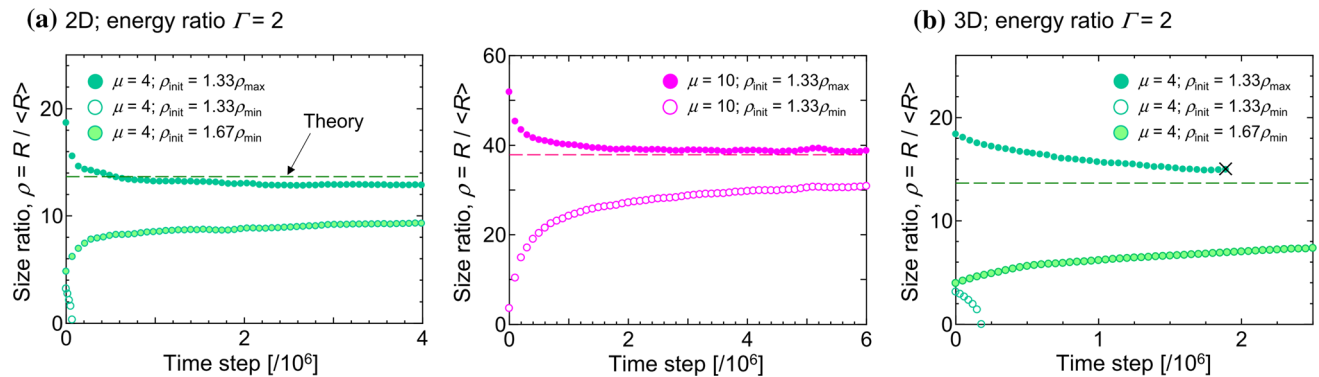
Figure 6 Temporal variations in size ratio ρ for **a** 2D system with energy ratio $\Gamma = 2$ and mobility ratios $\mu = 4$–10 and **b** 3D system with $\Gamma = 2$ and $\mu = 4$, as obtained for different initial size ratios, $\rho_{init} = 1.33\rho_{min}$ and $1.33\rho_{max}$. For comparison, the limiting values of ρ (i.e., ρ_{max}) predicted from the mean-field theory [17] are also given. The cross mark in (**b**) indicates the termination of the simulation because the specific grain reached the boundaries of the computational domain. In (**b**) and the left-hand panel of (**a**), in contrast to the theoretical prediction, the specific grains shrink and disappear for $\rho_{init} = 1.33\rho_{min}$; for these cases, additional simulations using a slightly larger initial size, $\rho_{init} = 1.67\rho_{min}$, were performed.
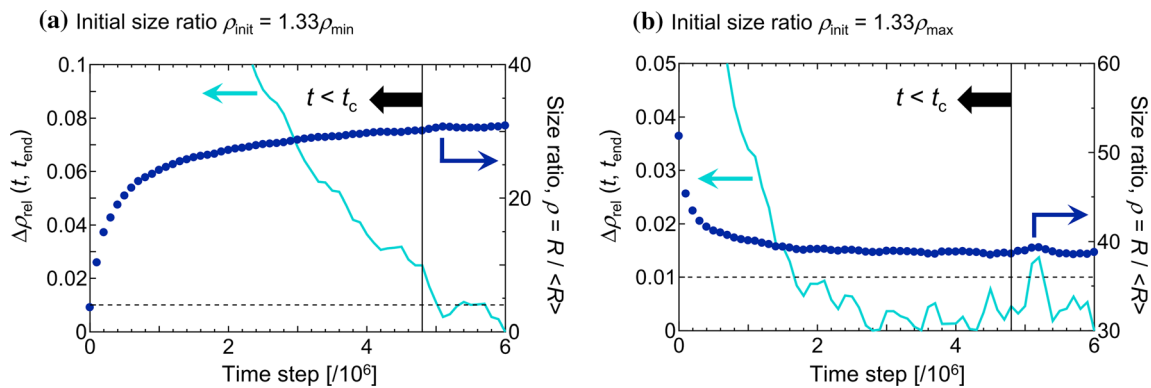
Figure 7 Temporal variations in size ratio ρ and relative change $\Delta\rho_{rel}(t, t_{end})$, as obtained for 2D abnormal grain growth at $\Gamma = 2$, $\mu = 10$ and different initial size ratios: **a** $\rho_{init} = 1.33\rho_{min}$ and **b** $\rho_{init} = 1.33\rho_{max}$.

values smaller than $\varepsilon = 0.01$ are observed only near t_{end} (i.e., $t > t_c$). Hence, the results were judged to converge incompletely. By contrast, for the case of $\rho_{init} = 1.33\rho_{max}$ (Fig. 7b), $\Delta\rho_{rel}(t, t_{end})$ becomes smaller than $\varepsilon = 0.01$ at around $t = 2 \times 10^6$ time steps, which is in the period $t < t_c$. Subsequently, the temporal variation in ρ is rather stable, and therefore, the result can be considered to have converged completely. Hereafter, incompletely converged results are noted accordingly in the main text and figures.

Next, we compared the simulation and theoretical results in greater detail by plotting the simulated temporal variations in ρ onto the theoretical diagram of abnormal grain growth conditions (Fig. 2) for all conditions of ρ_{init}, Γ, and μ that are summarized in Sect. 3.2.1 and schematically illustrated in Fig. 4. The results for 2D and 3D simulations are shown in Figs. 8 and 9, respectively. An increase in the ρ value from the initial value (i.e., $d\rho/dt > 0$: abnormal grain growth occurs) is indicated by the upward arrows near the plots, whereas a decrease in the ρ value (i.e., $d\rho/dt < 0$: no abnormal growth occurs) is indicated by the downward arrows. Furthermore, among the results corresponding to the growth or abnormal growth of a specific grain, the incompletely converged results, as determined from Eqs. (13)–(14), are denoted by asterisks near the upward/downward arrows.

The 2D simulation results (Fig. 8) show good agreement with the mean-field theory on the occurrence of abnormal growth. For the conditions where no abnormal growth is expected ($\rho_{init} = 0.67\rho_{min}$ for $\Gamma < \mu$ and $\rho_{init} = 4$ for $\Gamma > \mu$), the specific grains in
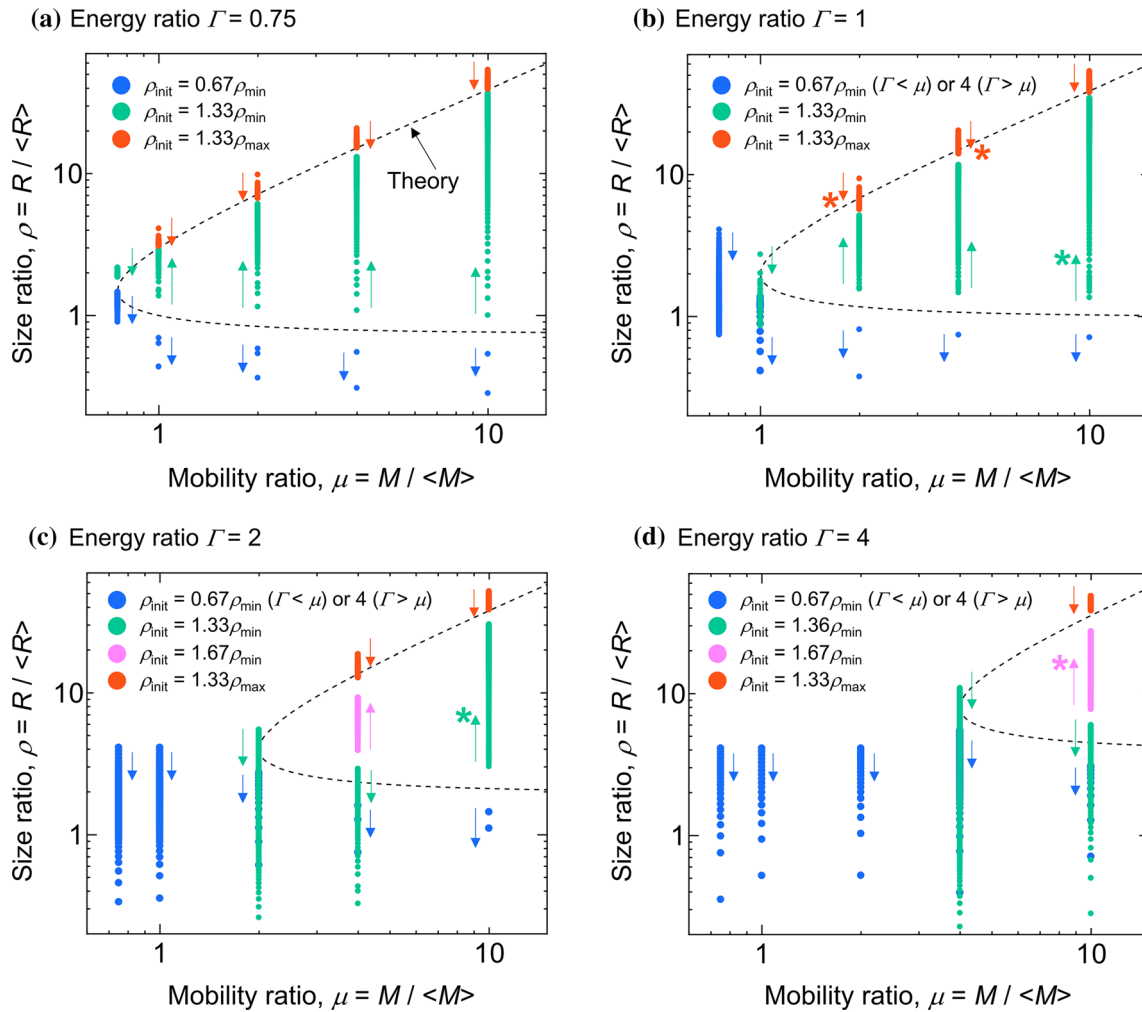
Figure 8 Temporal variations in size ratio ρ as functions of ρ_{init} and μ for 2D abnormal grain growth compared to the theoretical diagram shown in Fig. 2: **a** $\Gamma = 0.75$, **b** $\Gamma = 1$, **c** $\Gamma = 2$, and **d** $\Gamma = 4$. The increase in the ρ value from the initial value (i.e., $d\rho/dt > 0$: abnormal grain growth occurs) is indicated by upward arrows near the plots, whereas the decrease in the ρ value (i.e., $d\rho/dt < 0$: no abnormal growth occurs) is indicated by downward arrows. Incompletely converged results, as determined from Eqs. (13)–(14), are denoted with asterisks near the arrows. In some results shown in the panels (c) and (d), in contrast to the theoretical prediction, the specific grain does not abnormally grow, but shrinks and disappears for the condition of $\rho_{init} = 1.33\rho_{min}$; for these cases, additional simulations using slightly larger initial relative size, $\rho_{init} = 1.67\rho_{min}$, were performed.

the simulations decrease in their relative sizes. Furthermore, for the conditions of growth ($\rho_{init} = 1.33\rho_{max}$) and abnormal growth ($\rho_{init} = 1.33\rho_{min}$), most simulations show that the ρ value of the specific grain approaches the limiting value predicted by the mean-field theory (upper bounds of the theoretical curves), although a few results do not completely converge. At $\Gamma = 2$ with $\mu = 4$ (Fig. 8c) and $\Gamma = 4$ with $\mu = 10$ (Fig. 8d), the specific grain with an initial size of $\rho_{init} = 1.33\rho_{min}$ does not undergo abnormal growth, but shrinks, which contradicts the theory. However, at a slightly larger value of $\rho_{init} = 1.67\rho_{min}$, the specific grains grow abnormally to the theoretical

ρ_{max} value. In addition, in some cases, ρ converges to somewhat smaller values than those predicted theoretically (e.g., the results for $\Gamma = 1$ with $\mu = 2$, 4 and $\Gamma = 2$ with $\mu = 4$); this is particularly evident in the cases where the initial size ratio is smaller than the limiting size (i.e., $\rho_{init} = 1.33\rho_{min}$ or $1.67\rho_{min}$). However, the magnitudes of the relative errors for the limiting ρ values between the simulation and theoretical results are all less than 30%.

In the 3D simulation results in Fig. 9, although the temporal variation in ρ does not fully converge in several cases, there is a clear indication that the simulation and theoretical predictions are in good
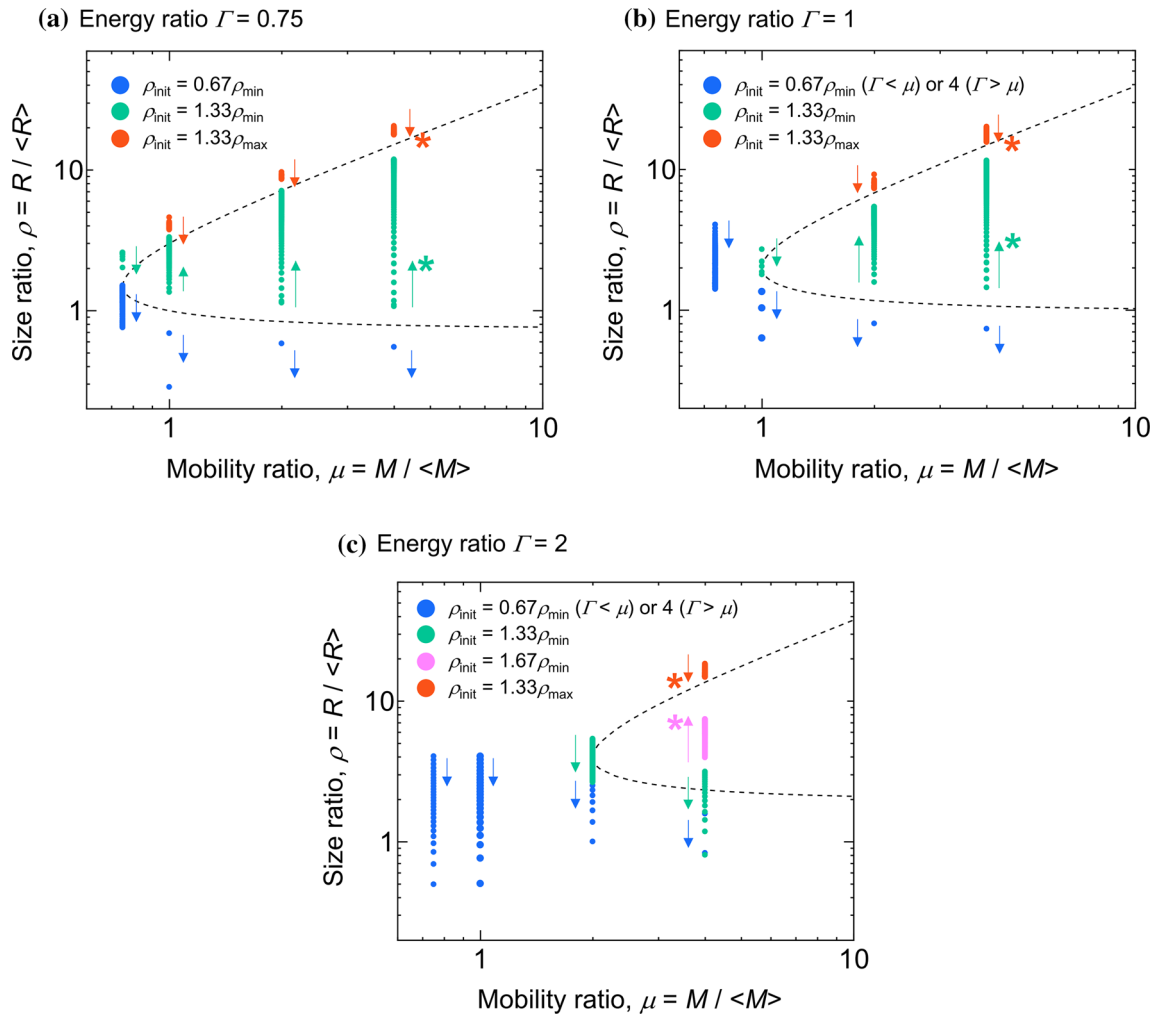
Figure 9 Temporal variations in size ratio ρ as functions of ρ_{init} and μ for 3D abnormal grain growth compared to the theoretical diagram shown in Fig. 2: **a** $\Gamma = 0.75$, **b** $\Gamma = 1$, and **c** $\Gamma = 2$. The meanings of the symbols are the same as those in Fig. 8.

agreement in terms of the occurrence of abnormal growth and limiting size attained by the abnormally growing grains. That is, for the conditions where abnormal growth is not expected to occur ($\rho_{init} = 0.67\rho_{min}$ for $\Gamma < \mu$ and $\rho_{init} = 4$ for $\Gamma > \mu$), the simulated ρ values decrease. For the conditions of growth ($\rho_{init} = 1.33\rho_{max}$) and abnormal growth ($\rho_{init} = 1.33\rho_{min}$), most of the simulated ρ values approach the theoretical values, with the only exception being the result for $\Gamma = 2, \mu = 4$, and $\rho_{init} = 1.33\rho_{min}$ previously shown in Fig. 6b.

The results summarized above demonstrated that the mean-field theory generally describes the simulated abnormal grain growth for both 2D and 3D systems well. The small deviations between the simulation and theoretical results can be partially attributed to the incomplete convergence of ρ in some cases, particularly for the 3D cases. However, even in the current 2D simulations where the temporal variations in ρ at later stages were very small (relative changes in ρ values were all smaller than 3% during the last 10^6 steps of the simulations), slight deviations were still observed. Therefore, physical factors must cause the deviations that are more dominant than the incomplete convergence of ρ. The possible reasons for these deviations are discussed below.

Possible sources of the deviations between theoretical and simulation results

This section examines the causes of the small discrepancies between the simulation and mean-field theoretical results, which were observed for $\Gamma \geq 2$ and for the simulations starting from the initial size

ratio smaller than ρ_{max} (i.e., $\rho_{init} = 1.33\rho_{min}$ or $1.67\rho_{min}$). The major source of the slight deviations is probably the inaccuracies of the basic equations used in the derivation of the mean-field theory. As mentioned in Sect. 2, the theory was derived using parabolic law (Eq. 2) for the growth kinetics of the matrix grains, and the mean-field equation (Eq. 1) for specific grain kinetics. In the former, the squared average size of the matrix, $\langle R \rangle^2$, increases linearly with time at a slope of $0.5\alpha\langle M \rangle\langle\gamma\rangle$ ($\alpha = 0.5$: geometrical constant), whereas the latter predicts that the growth rate, RdR/dt, of a specific grain is a linear function of its relative size ρ with a slope of $\alpha M\langle\gamma\rangle$. Herein, we tested the accuracies of these equations by comparing them with simulations. We used the 2D simulation results because the convergence of the abnormal growth kinetics was better in the 2D simulations than in the 3D simulations, as confirmed in the previous section.

In Fig. 10, we plotted the $\langle R \rangle^2$ vs. time and RdR/dt vs. ρ curves from a 2D simulation, comparing their slopes with the theoretical ones. Here, as the simulated results, those for the condition of $\Gamma = 2$ and $\mu = 4$ shown in Fig. 8c were used; this is because, as described above, relatively large deviations between the simulation and theory were observed for this condition. Plots with different colors indicate the simulations starting from different initial size ratios, $\rho_{init} = 1.67\rho_{min}$ and $\rho_{init} = 1.33\rho_{max}$. From Fig. 10a, we can see that $\langle R \rangle^2$ linearly increases with time as predicted by Eq. (2), exhibiting almost identical

results for $\rho_{init} = 1.67\rho_{min}$ and $1.33\rho_{max}$. However, the slopes of the linear fit curves, 0.271 and 0.275, are somewhat larger than that of the parabolic law, 0.5α $\langle M \rangle\langle\gamma\rangle = 0.5 \times 0.5 \times 1 \times 1 = 0.25$, with the relative error being 8–10%. Note that the slope larger than the theoretical value of the parabolic law has been frequently reported from the previous simulations for normal grain growth using various numerical models (e.g., Monte Carlo model [79, 80], cellular automaton model [81, 82], vertex model [83, 84], etc.), and therefore, this disagreement between the simulation and theory comes from the inaccuracy in the theory, not in the simulation.

As shown in Fig. 10b, although the RdR/dt vs. ρ curves exhibit large scatters, a linear tendency is observed for both $\rho_{init} = 1.67\rho_{min}$ and $1.33\rho_{max}$ in accordance with the mean-field equation (Eq. 1). The slopes of the fitted curves are 1.760 for $\rho_{init} = 1.67\rho_{min}$ and 1.985 for $\rho_{init} = 1.33\rho_{max}$. While the latter case (the specific grain initially larger than the limiting size ρ_{max}) shows quite a good agreement with the assumed value of $\alpha M\langle\gamma\rangle = 0.5 \times 4 \times 1 = 2$ in Eq. (1), the former case (the specific grain initially smaller than ρ_{max}) yields a relatively large error of $\sim 12\%$. This implies that the mean-field equation is less valid for the conditions where the specific grain size is relatively small, which resulted in the visible deviations between the simulation and theory observed for $\rho_{init} = 1.33\rho_{min}$ or $1.67\rho_{min}$ (see Figs. 6 and 8). What causes this inaccuracy of the mean-field equation for a small grain size is probably the assumption used in
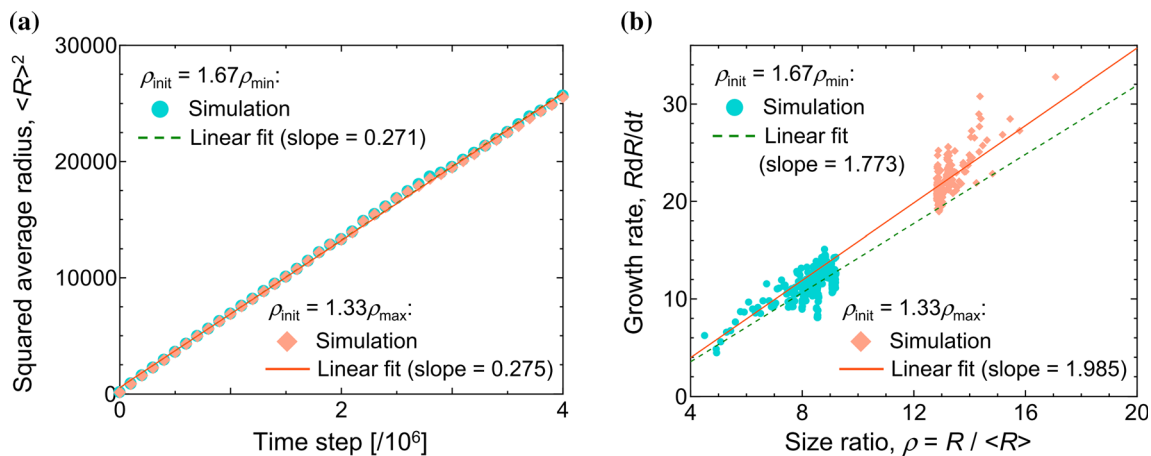

Figure 10 a Temporal variation in the squared average size $\langle R \rangle^2$ of the matrix grains and **b** growth rate RdR/dt of the specific grain as a function of size ratio $\rho = R/\langle R \rangle$, as calculated from the 2D simulations with $\Gamma = 2$ and $\mu = 4$ starting from $\rho_{init} = 1.67\rho_{min}$ and $\rho_{init} = 1.33\rho_{max}$, which correspond to the results shown in Fig. 8c.

the equation. That is, the mean-field equation assumes that the growth rate of a given grain is determined by the interaction between its own field (its size, R) and the mean field (average size of matrix grains, $\langle R \rangle$). However, as Kim et al. [50] pointed out, the growth rate of a given grain is in fact governed by its own field and local field (average size of its neighboring grains), rather than the mean field. Therefore, the applicability of the mean-field equation depends on how accurately the mean field approximates the local field. The approximation will be improper for relatively small grains with a small number of neighbors, because with decreasing neighboring grains the local field statistically deviates from the mean field. In the current simulations for $\Gamma = 2$ and $\mu = 4$, the number of neighboring grains of the specific grain was observed to converge with time to around 45 in the case of $\rho_{init} = 1.33\rho_{max}$ and around 30 in the case of $\rho_{init} = 1.67\rho_{min}$. Therefore, for the condition of $\rho_{init} = 1.67\rho_{min}$, the abnormal growth behavior of the specific grain would be inherently difficult to approach that of the mean-field theory, compared to the case of $\rho_{init} = 1.33\rho_{max}$.

The above results conclude that the basic equations actually include some errors particularly when the initial relative size ρ_{init} of the specific grain is smaller than the limiting value ρ_{max} (i.e., $\rho_{init} = 1.33\rho_{min}$ or $1.67\rho_{min}$). The deviations between the simulation and mean-field theory of abnormal growth are attributable to the basic equations. Hence, the prediction accuracy of the abnormal grain growth could be improved by reformulating the mean-field theory using more sophisticated basic equations for individual and average grain growth kinetics, such as those proposed in Refs. [85, 86] capable of accounting for the local field as well as the mean field. However, given the notable simplicity of the current mean-field theory, its overall prediction accuracy would be acceptable and sufficiently high.

Conclusions

This study was conducted to elucidate the validity of the mean-field theory of abnormal grain growth via very large-scale 2D and 3D phase-field simulations. Utilizing the MPF model and parallel GPU computing, a series of large-scale simulations with several hundreds of thousands of grains were performed while varying the size ratio $\rho = R/\langle R \rangle$, boundary

energy ratio $\Gamma = \gamma/\langle\gamma\rangle$, and mobility ratio $\mu = M/\langle M \rangle$ between the specific grain and matrix grains, through which the simulated results and theoretical predictions on the abnormal grain growth behaviors were compared in detail. The comparisons showed that the mean-field theory generally agrees well with the simulated results for both 2D and 3D systems, in terms of whether the abnormal growth of the specific grain occurs or not as well as the limiting size that the abnormally growing grain reaches. Relatively large deviations between the simulation and theory were observed for the conditions with energy ratio $\Gamma > 1$ and initially small relative size ρ, which is mainly attributable to inaccuracies of the two basic equations (Eqs. 1 and 2) used in the derivation of the mean-field theory. However, the magnitude of relative error for the limiting grain size is at most less than 30%, and given the notable simplicity of the current mean-field theory, its overall prediction accuracy would be acceptably high.

In the previous studies so far, the validation of the mean-field theory has been done only for limited samples in a qualitative or semiquantitative manner. The systematic, large-scale MPF simulations presented here first clarified the accuracy of the mean-field theory for various conditions of grain size and grain boundary properties, providing quantitative evidence that the theory is a versatile and fairly accurate framework for abnormal grain growth prediction despite its notable simplicity. Moreover, the accuracy of the mean-field theory is expected to be further improved if necessary by modifying its basic equations. These findings will provide a useful platform for analytically modeling abnormal grain growth and for interpreting actual experimental results based on the analytical approach.

Finally, we discuss some remarks on future work. In this study, even using the present large-scale computations, it was found difficult to determine the conclusive values for the limiting size of abnormal grains in 3D systems. This problem could be resolved by the S-PFM model developed in the recent work of Dimokrati et al. [87]; this model can simulate grain growth accurately using very coarse grid spacing and, therefore, has a potential to drastically enlarge computational scales. In addition, the current work did not consider the misorientation (and inclination) dependencies of grain boundary energy and mobility due to the lack of accurate models for the anisotropic boundary properties. Our ongoing project is

attempting to solve this problem based on data assimilation technique [88–90], which will allow for extracting large datasets of grain boundary properties via the integration of observation data of grain growth (experiments or atomistic calculations) into phase-field simulations and thereby constructing accurate models for misorientation-dependent boundary properties. Thus, using these cutting-edge techniques, our future work will study the effects of nonuniform boundary properties on abnormal grain growth for further enlarged 3D systems with more realistic conditions of grain boundary properties. We believe that the findings presented here will also hold for such more realistic and enlarged systems.

Acknowledgements

Authors contributions

EM was responsible for conceptualization, methodology, software, investigation, formal analysis, visualization, writing the original draft, writing, reviewing, and editing, and funding acquisition. MO, YS, and AY were involved in conceptualization, methodology, and writing, reviewing, and editing. TT had contributed to conceptualization, methodology, software, writing, review, and editing, funding acquisition, supervision, and project administration.

Data availability

The raw/processed data supporting the findings of this study are available upon reasonable request.

Declarations

Conflict of interest The authors declare that there are no conflicts of interest.

References

[1] Humphreys FJ, Hatherly M (2004) Recrystallisation and related annealing phenomena, 2nd edn. Elsevier Ltd., Oxford

[2] Atkinson HV (1988) Overview no. 65: Theories of normal grain growth in pure single phase systems. Acta Metall 36:469–491. https://doi.org/10.1016/0001-6160(88)90079-X

[3] Rollett AD (2004) Crystallographic texture change during grain growth. JOM 56:63–68. https://doi.org/10.1007/s11837-004-0075-9

[4] Lee HY, Kim JS, Kim DY (2000) Fabrication of BaTiO3 single crystals using secondary abnormal grain growth. J Eur Ceram Soc 20:1595–1597. https://doi.org/10.1016/s0955-2219(00)00030-3

[5] Kusama T, Omori T, Saito T et al (2017) Ultra-large single crystals by abnormal grain growth. Nat Commun 8:1–8. https://doi.org/10.1038/s41467-017-00383-0

[6] Hillert M (1965) On the theory of normal and abnormal grain growth. Acta Metall 13:227–238. https://doi.org/10.1017/CBO9781107415324.004

[7] Anderson I, Grong Ø, Ryum N (1995) Analytical modelling of grain growth in metals and alloys in the presence of growing and dissolving precipitates—II. Abnormal grain growth. Acta Metall Mater 43:2689–2700

[8] Thompson CV (2000) Structure evolution during processing of polycrystalline films. Annu Rev Mater Sci 30:159–190

[9] Longworth HP, Thompson CV (1991) Abnormal grain growth in aluminum alloy thin films. J Appl Phys 69:3929–3940. https://doi.org/10.1063/1.348452

[10] Holm EA, Miodownik MA, Rollett AD (2003) On abnormal subgrain growth and the origin of recrystallization nuclei. Acta Mater 51:2701–2716. https://doi.org/10.1016/S1359-6454(03)00079-X

[11] Rohrer GS (2011) Grain boundary energy anisotropy: a review. J Mater Sci 46:5881–5895. https://doi.org/10.1007/s10853-011-5677-3

[12] Dillon SJ, Harmer MP, Luo J (2009) Grain boundary complexions in ceramics and metals: an overview. JOM 61:38–44. https://doi.org/10.1007/s11837-009-0179-3

[13] Frazier WE, Rohrer GS, Rollett AD (2015) Abnormal grain growth in the Potts model incorporating grain boundary complexion transitions that increase the mobility of individual boundaries. Acta Mater 96:390–398. https://doi.org/10.1016/j.actamat.2015.06.033

[14] Simpson CJ, Aust KT, Winegard WC (1971) The four stages of grain growth. Metall Trans 2:987–991. https://doi.org/10.1007/BF02664229

[15] Riontino G, Antonione C, Battezzati L et al (1979) Kinetics of abnormal grain growth in pure iron. J Mater Sci 14:86–90. https://doi.org/10.1007/BF01028331

[16] Dennis J, Bate PS, Humphreys JF (2007) Abnormal grain growth in metals. Mater Sci Forum 558–559:717–722. https://doi.org/10.4028/www.scientific.net/msf.558-559.717

[17] Humphreys FJ (1997) A unified theory of recovery, recrystallization and grain growth, based on the stability and growth of cellular microstructures—I. The basic model. Acta Mater 45:4231–4240. https://doi.org/10.1016/S1359-6454(97)00070-0

[18] Na SM, Flatau AB (2013) Global Goss grain growth and grain boundary characteristics in magnetostrictive Galfenol sheets. Smart Mater Struct 22:125026. https://doi.org/10.1088/0964-1726/22/12/125026

[19] Humphreys FJ (1997) A unified theory of recovery, recrystallization and grain growth, based on the stability and growth of cellular microstructures—II. The effect of second-phase particles. Acta Mater 45:5031–5039

[20] Rollett AD, Mullins WW (1997) On the growth of abnormal grains. Scr Mater 36:975–980. https://doi.org/10.1016/S1359-6462(96)00501-5

[21] Mullins WW (1956) Two-dimensional motion of idealized grain boundaries. J Appl Phys 27:900–904. https://doi.org/10.1063/1.1722511

[22] Ferry M, Humphreys FJ (1996) Discontinuous subgrain growth in deformed and annealed 110 ⟨001 aluminium single crystals. Acta Mater 44:1293–1308. https://doi.org/10.1016/S0921-5093(02)00748-7

[23] Charit I, Mishra RS, Mahoney MW (2002) Multi-sheet structures in 7475 aluminum by friction stir welding in concert with post-weld superplastic forming. Scr Mater 47:631–636. https://doi.org/10.1016/S1359-6462(02)00257-9

[24] Hassan KAA, Norman AF, Price DA, Prangnell PB (2003) Stability of nugget zone grain structures in high strength Al-alloy friction stir welds during solution treatment. Acta Mater 51:1923–1936. https://doi.org/10.1016/S1359-6454(02)00598-0

[25] Yu CY, Sun PL, Kao PW, Chang CP (2004) Evolution of microstructure during annealing of a severely deformed aluminum. Mater Sci Eng A 366:310–317. https://doi.org/10.1016/j.msea.2003.08.039

[26] Ferry M, Hamilton NE, Humphreys FJ (2005) Continuous and discontinuous grain coarsening in a fine-grained particle-containing Al-Sc alloy. Acta Mater 53:1097–1109. https://doi.org/10.1016/j.actamat.2004.11.006

[27] Charit I, Mishra RS (2008) Abnormal grain growth in friction stir processed alloys. Scr Mater 58:367–371. https://doi.org/10.1016/j.scriptamat.2007.09.052

[28] Young JP, Askari H, Hovanski Y et al (2015) Thermal microstructural stability of AZ31 magnesium after severe plastic deformation. Mater Charact 101:9–19. https://doi.org/10.1016/j.matchar.2014.12.026

[29] Uttarasak K, Chongchitnan W, Matsuda K et al (2019) Evolution of Fe-containing intermetallic phases and abnormal grain growth in 6063 aluminum alloy during homogenization. Results Phys 15:102535. https://doi.org/10.1016/j.rinp.2019.102535

[30] Agnoli A, Bernacki M, Logé R et al (2015) Selective growth of low stored energy grains during δ sub-solvus annealing in the Inconel 718 nickel-based superalloy. Metall Mater Trans A Phys Metall Mater Sci 46:4405–4421. https://doi.org/10.1007/s11661-015-3035-9

[31] Weygand D, Bréchet Y, Lépinoux J (2001) Mechanisms and kinetics of recrystallisation: a two dimensional vertex dynamics simulation. Interface Sci 9:311–317. https://doi.org/10.1023/A:1015175231826

[32] Hurley PJ, Humphreys FJ (2003) Modelling the recrystallization of single-phase aluminium. Acta Mater 51:3779–3793. https://doi.org/10.1016/S1359-6454(03)00192-7

[33] Radhakrishnan B, Sarma G (2004) Simulating the deformation and recrystallization of aluminum bicrystals. JOM 56:55–62. https://doi.org/10.1007/s11837-004-0074-x

[34] Zurob HS, Bréchet Y, Dunlop J (2006) Quantitative criterion for recrystallization nucleation in single-phase alloys: prediction of critical strains and incubation times. Acta Mater 54:3983–3990. https://doi.org/10.1016/j.actamat.2006.04.028

[35] Suwa Y, Saito Y, Onodera H (2007) Phase field simulation of stored energy driven interface migration at a recrystallization front. Mater Sci Eng A 457:132–138. https://doi.org/10.1016/j.msea.2007.01.091

[36] Després A, Greenwood M, Sinclair CW (2020) A mean-field model of static recrystallization considering orientation spreads and their time-evolution. Acta Mater 199:116–128. https://doi.org/10.1016/j.actamat.2020.08.013

[37] Srolovitz DJ, Grest GS, Anderson MP (1985) Computer simulation of grain growth-V. Abnormal grain growth. Acta

Metall 33:2233–2247. https://doi.org/10.1016/0001-6160(85)90185-3

[38] Rollett AD, Srolovitz DJ, Anderson MP (1989) Simulation and theory of abnormal grain growth-Anisotropic grain boundary energies and mobilities. Acta Metall 37:1227–1240

[39] Vertyagina Y, Mahfouf M (2014) A 3D cellular automata model of the abnormal grain growth in austenite. J Mater Sci 50:745–754. https://doi.org/10.1007/s10853-014-8634-0

[40] Suwa Y, Saito Y, Onodera H (2007) Phase-field simulation of abnormal grain growth due to inverse pinning. Acta Mater 55:6881–6894. https://doi.org/10.1016/j.actamat.2007.08.045

[41] Liu Y, Militzer M, Perez M (2019) Phase field modelling of abnormal grain growth. Materials (Basel) 12:4048. https://doi.org/10.3390/MA12244048

[42] Kinoshita T, Ohno M (2020) Phase-field simulation of abnormal grain growth during carburization in Nb-added steel. Comput Mater Sci 177:109558. https://doi.org/10.1016/j.commatsci.2020.109558

[43] Zhang Y, Liu L (2021) Phase field simulation of abnormal grain growth mediated by initial particle size distribution. Adv Powder Technol 32:3395–3404. https://doi.org/10.1016/j.apt.2021.07.025

[44] Pei R, Korte-Kerzel S, Al-Samman T (2020) Normal and abnormal grain growth in magnesium: experimental observations and simulations. J Mater Sci Technol 50:257–270. https://doi.org/10.1016/j.jmst.2020.01.014

[45] Steinbach I, Pezzolla F, Nestler B et al (1996) A phase field concept for multiphase systems. Physica D 94:135–147

[46] Fan D, Chen L-Q (1997) Computer simulation of grain growth using a continuum field model. Acta Mater 45:611–622

[47] Garcke H, Nestler B, Stoth B (1999) A multiphase field concept: numerical simulations of moving phase boundaries and multiple junctions. SIAM J Appl Math 60:295–315. https://doi.org/10.1137/S0036139998334895

[48] Steinbach I, Pezzolla F (1999) A generalized field method for multiphase transformations using interface fields. Physica D 134:385–393

[49] Tóth GI, Pusztai T, Gránásy L (2015) Consistent multiphase-field theory for interface driven multidomain dynamics. Phys Rev B 92:184105. https://doi.org/10.1103/PhysRevB.92.184105

[50] Kim SG, Kim DI, Kim WT, Park YB (2006) Computer simulations of two-dimensional and three-dimensional ideal grain growth. Phys Rev E 74:061605. https://doi.org/10.1103/PhysRevE.74.061605

[51] Gruber J, Ma N, Wang Y et al (2006) Sparse data structure and algorithm for the phase field method. Model Simul Mater Sci Eng 14:1189–1195. https://doi.org/10.1088/0965-0393/14/7/007

[52] Vedantam S, Patnaik BSV (2006) Efficient numerical algorithm for multiphase field simulations. Phys Rev E 73:016703. https://doi.org/10.1103/PhysRevE.73.016703

[53] Moelans N, Wendler F, Nestler B (2009) Comparative study of two phase-field models for grain growth. Comput Mater Sci 46:479–490. https://doi.org/10.1016/j.commatsci.2009.03.037

[54] Miyoshi E, Takaki T, Ohno M, Shibuta Y (2020) Accuracy evaluation of phase-field models for grain growth simulation with anisotropic grain boundary properties. ISIJ Int 60:160–167. https://doi.org/10.2355/isijinternational.isijint-2019-305

[55] Shimokawabe T, Takaki T, Endo T et al (2011) Peta-scale phase-field simulation for dendritic solidification on the TSUBAME 2.0 supercomputer. In: Proceedings of 2011 International conference for high performance computing, networking, storage and analysis. ACM, Seattle, pp 1–11

[56] Shibuta Y, Ohno M, Takaki T (2018) Advent of cross-scale modeling: high-performance computing of solidification and grain growth. Adv Theory Simul 1:1800065. https://doi.org/10.1002/adts.201800065

[57] Mitsuyama Y, Takaki T, Sakane S et al (2020) Permeability tensor for columnar dendritic structures: Phase–field and lattice Boltzmann study. Acta Mater 188:282–287. https://doi.org/10.1016/j.actamat.2020.02.016

[58] Takaki T, Sakane S, Ohno M et al (2020) Large-scale phase-field lattice Boltzmann study on the effects of natural convection on dendrite morphology formed during directional solidification of a binary alloy. Comput Mater Sci 171:109209. https://doi.org/10.1016/j.commatsci.2019.109209

[59] Takaki T, Sakane S, Ohno M et al (2022) Phase-field study on an array of tilted columnar dendrites during the directional solidification of a binary alloy. Comput Mater Sci 203:111143. https://doi.org/10.1016/j.commatsci.2021.111143

[60] Miyoshi E, Takaki T, Ohno M et al (2017) Ultra-large-scale phase-field simulation study of ideal grain growth. npj Comput Mater 3:25. https://doi.org/10.1038/s41524-017-0029-8

[61] Miyoshi E, Takaki T, Ohno M et al (2019) Large-scale phase-field simulation of three-dimensional isotropic grain growth in polycrystalline thin films. Model Simul Mater Sci Eng 27:054003. https://doi.org/10.1088/1361-651X/ab1e8b

[62] Miyoshi E, Takaki T, Sakane S et al (2021) Large-scale phase-field study of anisotropic grain growth: effects of misorientation-dependent grain boundary energy and

mobility. Comput Mater Sci 186:109992. https://doi.org/10.1016/j.commatsci.2020.109992

[63] Kirch DM, Jannot E, Barrales-Mora LA et al (2008) Inclination dependence of grain boundary energy and its impact on the faceting and kinetics of tilt grain boundaries in aluminum. Acta Mater 56:4998–5011. https://doi.org/10.1016/j.actamat.2008.06.017

[64] Bulatov VV, Reed BW, Kumar M (2014) Grain boundary energy function for fcc metals. Acta Mater 65:161–175. https://doi.org/10.1016/j.actamat.2013.10.057

[65] Thompson CV, Frost HJ, Spaepen F (1987) The relative rates of secondary and normal grain growth. Acta Metall 35:887–890

[66] Gottstein G, Molodov DA, Shvindlerman LS et al (2001) Grain boundary migration: misorientation dependence. Curr Opin Solid State Mater Sci 5:9–14. https://doi.org/10.1016/S1359-0286(00)00030-9

[67] Olmsted DL, Holm EA, Foiles SM (2009) Survey of computed grain boundary properties in face-centered cubic metals-II: Grain boundary mobility. Acta Mater 57:3704–3713. https://doi.org/10.1016/j.actamat.2009.04.015

[68] Zhang J, Ludwig W, Zhang Y et al (2020) Grain boundary mobilities in polycrystals. Acta Mater 191:211–220. https://doi.org/10.1016/j.actamat.2020.03.044

[69] Takaki T, Hirouchi T, Hisakuni Y et al (2008) Multi-phase-field model to simulate microstructure evolutions during dynamic recrystallization. Mater Trans 49:2559–2565. https://doi.org/10.2320/matertrans.MB200805

[70] Ko K, Cha P, Srolovitz DJ, Hwang N (2009) Abnormal grain growth induced by sub-boundary-enhanced solid-state wetting: analysis by phase-field model simulations. Acta Mater 57:838–845. https://doi.org/10.1016/j.actamat.2008.10.030

[71] Olmsted DL, Foiles SM, Holm EA (2009) Survey of computed grain boundary properties in face-centered cubic metals: I. Grain boundary energy. Acta Mater 57:3694–3703. https://doi.org/10.1016/j.actamat.2009.04.007

[72] Petrov R, Kestens L, Verbeken K, Houbaert Y (2004) Grain growth after intercritical rolling. Mater Sci Forum 467–470:305–310. https://doi.org/10.4028/www.scientific.net/msf.467-470.305

[73] Lu N, Kang J, Shahani AJ (2021) Origins of non-random particle distributions and implications to abnormal grain growth in an Al-3.5 Wt Pct Cu Alloy. Metall Mater Trans A Phys Metall Mater Sci 52:914–927. https://doi.org/10.1007/s11661-020-06125-0

[74] Furubayashi E (1970) An origin of the recrystallized grains with preferred orientations in cold rolled Fe-3% Si Alloy. Trans Iron Steel Inst Jpn 9:222–238. https://doi.org/10.2355/tetsutohagane1955.56.6_734

[75] Hutchinson B (2012) Origin of Goss texture during secondary recrystallisation in silicon-steel. Mater Sci Forum 715–716:73–80. https://doi.org/10.4028/www.scientific.net/MSF.715-716.73

[76] DeCost BL, Holm EA (2017) Phenomenology of abnormal grain growth in systems with nonuniform grain boundary mobility. Metall Mater Trans A Phys Metall Mater Sci 48:2771–2780. https://doi.org/10.1007/s11661-016-3673-6

[77] Kundin J, Almeida RSM, Salama H et al (2020) Phase-field simulation of abnormal anisotropic grain growth in polycrystalline ceramic fibers. Comput Mater Sci 185:109926. https://doi.org/10.1016/j.commatsci.2020.109926

[78] Miyoshi E, Takaki T, Ohno M et al (2018) Correlation between three-dimensional and cross-sectional characteristics of ideal grain growth: large-scale phase-field simulation study. J Mater Sci 53:15165–15180. https://doi.org/10.1007/s10853-018-2680-y

[79] Anderson MP, Srolovitz DJ, Grest GS, Sahni PS (1984) Computer simulation of grain growth—I. Kinetics. Acta Metall 32:783–791. https://doi.org/10.1016/0001-6160(84)90151-2

[80] Upmanyu M, Hassold GN, Kazaryan A et al (2002) Boundary mobility and energy anisotropy effects on microstructural evolution during grain growth. Interface Sci 10:201–216. https://doi.org/10.1023/A:1015832431826

[81] Geiger J, Roósz A, Barkóczy P (2001) Simulation of grain coarsening in two dimensions by Cellular-Automaton. Acta Mater 49:623–629. https://doi.org/10.1016/S1359-6454(00)00352-9

[82] He Y, Ding H, Liu L, Shin K (2006) Computer simulation of 2D grain growth using a cellular automata model based on the lowest energy principle. Mater Sci Eng A 429:236–246. https://doi.org/10.1016/j.msea.2006.05.070

[83] Frost H, Thompson CV, Howe CL, Whang J (1988) A two-dimensional computer simulation of capillarity-driven grain growth: preliminary results. Scr Metall 22:65–70

[84] Mason JK, Lazar EA, MacPherson RD, Srolovitz DJ (2015) Geometric and topological properties of the canonical grain growth microstructure. Phys Rev E 92:063308. https://doi.org/10.1103/PhysRevE.92.063308

[85] Zöllner D, Streitenberger P (2006) Three-dimensional normal grain growth: Monte Carlo Potts model simulation and analytical mean field theory. Scr Mater 54:1697–1702. https://doi.org/10.1016/j.scriptamat.2005.12.042

[86] Breithaupt T, Hansen LN, Toppaladoddi S, Katz RF (2021) The role of grain-environment heterogeneity in normal grain growth: a stochastic approach. Acta Mater 209:116699. https://doi.org/10.1016/j.actamat.2021.116699

[87] Dimokrati A, Le Bouar Y, Benyoucef M, Finel A (2020) S-PFM model for ideal grain growth. Acta Mater 201:147–157. https://doi.org/10.1016/j.actamat.2020.09.073

[88] Yamanaka A, Maeda Y, Sasaki K (2019) Ensemble Kalman filter-based data assimilation for three-dimensional multi-phase-field model: estimation of anisotropic grain boundary properties. Mater Des 165:107577. https://doi.org/10.1016/j.matdes.2018.107577

[89] Miyoshi E, Ohno M, Shibuta Y et al (2021) Novel estimation method for anisotropic grain boundary properties based on Bayesian data assimilation and phase-field simulation. Mater Des 210:110089. https://doi.org/10.1016/j.matdes.2021.110089

[90] Ishii A, Yamanaka A, Miyoshi E et al (2021) Estimation of solid-state sintering and material parameters using phase-field modeling and ensemble four-dimensional variational method. Model Simul Mater Sci Eng 29:065012. https://doi.org/10.1088/1361-651X/ac13cd